JACS
JOURNAL OF THE AMERICAN CHEMICAL SOCIETY
Article
pubs.acs.org/JACS

Core–Satellites Assembly of Silver Nanoparticles on a Single Gold Nanoparticle via Metal Ion-Mediated Complex

Inhee Choi,[†,§,∥] Hyeon Don Song,[†,§] Suseung Lee,[†] Young In Yang,[†] Taewook Kang,*[,‡] and Jongheop Yi*[,†]

[†]World Class University Program of Chemical Convergence for Energy & Environment, School of Chemical and Biological Engineering, Institute of Chemical Processes, Seoul National University, Seoul 151-742, Republic of Korea

[‡]Department of Chemical and Biomolecular Engineering, Sogang University, Seoul, 121-742, Republic of Korea

Supporting Information

ABSTRACT: We report core–satellites (Au–Ag) coupled plasmonic nanoassemblies based on bottom-up, high-density assembly of molecular-scale silver nanoparticles on a single gold nanoparticle surface, and demonstrate direct observation and quantification of enhanced plasmon coupling (i.e., intensity amplification and apparent spectra shift) in a single particle level. We also explore metal ion sensing capability based on our coupled plasmonic core–satellites, which enabled at least 1000 times better detection limit as compared to that of a single plasmonic nanoparticle. Our results demonstrate and suggest substantial promise for the development of coupled plasmonic nanostructures for ultrasensitive detection of various biological and chemical analytes.

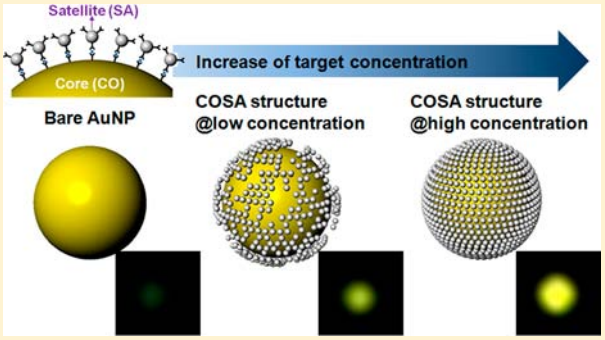

INTRODUCTION

Localized surface plasmon resonance (LSPR) of noble metal nanoparticles has been extensively explored, in attempts to develop platforms for the plasmonic sensing of biological and chemical analytes[1,2] as such plasmon resonances are sensitive to particle shape, size, composition, and the local refractive index surrounding nanoparticles. Plasmon band shifts caused by the specific binding of analyte molecules to ligand-modified nanoparticle surfaces are typically employed as optical sensing signals.[3−8] However, the majority of studies on LSPR-based methods to date, have been based on the interrogation of an ensemble of nanoparticles on a substrate[3−5] or in a solution[6−8] where obtained signals are averages from multiple nanoparticles with different sizes, and thus exhibit heterogeneous broadening, as compared to the signal from a single nanoparticle.[9,10] Extending LSPR sensing techniques to the level of a single nanoparticle,[9−13] as a result, could enable a highly sensitive optical sensing platform, because the absolute detection limit is directly associated with the number of analyte molecules per nanoparticle.

Nonetheless, single particle-based plasmonic detection methods show better sensing performances, but they are still limited by the resolution of spectral shift induced by a change in the dielectric property of particles' surroundings.[9,10] Therefore, in some cases, other strategies (i.e., plasmon resonance energy transfer[12,13] and plasmon coupling[14]) were explored to enhance the detection sensitivity. In particular, coupled plasmon nanoparticles offer promising and universal opportunities for developing new sensing platform, because plasmon resonances generated by such couplings could lead to the extremely strong intensity amplification as well as a readily distinctive spectral shift.

To date, several nanostructures to enable plasmon coupling have been demonstrated. Raspberry-type composites composed of a dielectric core and metallic satellites were fabricated, which showed plasmonic enhancement by plasmon coupling between gold particles in a shell layer while a core functioned simply as a support.[15] Many theoretical studies of coupled plasmonics also have been reported, including an investigation of the optical properties of heterodimers composed of a silver nanoparticle and a gold nanoparticle.[16] In addition, experimental efforts toward coupled plasmon nanoparticles, such as multimers (i.e., dimers[14,17,18] and trimers[17]) or simple core–satellite structures,[19] were reported via DNA-based assemblies. For example, sensing modality based on the actuation of discrete gold nanoparticle dimers was demonstrated by implementing target DNA-associated geometrical extension of the dimer.[18] Reconfigurable core–satellite structures were also experimentally demonstrated by DNA-linked nanoassembly[19−22] and theoretically studied by spectral simulation,[19,20,23] but have been limited to proof-of-concept demonstration with relatively large gold satellites assembled in a low density.

Herein, we report bottom-up, high-density assembly of molecular-scale silver nanoparticles on a single gold nanoparticle surface, enabling core–satellite (Au–Ag) coupled

Received: March 20, 2012
Published: June 29, 2012

   dx.doi.org/10.1021/ja302684w | J. Am. Chem. Soc. 2012, 134, 12083−12090

plasmon nanoparticles, and demonstrate direct observation and quantification of enhanced plasmon coupling (i.e., intensity amplification and apparent spectra shift) at a single particle level. We also explore metal ion sensing capability using our core−satellites nanostructures, which enabled at least 1000 times better detection limit as compared to that of single plasmonic nanoparticle.

RESULTS AND DISCUSSION

Our nanoassembly approach involves two steps: (1) the selective recognition of targets with the core nanoparticle and (2) targeted assembly with satellite nanoparticles, as schematically illustrated in Figure 1. A core nanoparticle with specific ligands is exposed to analytes to induce selective associations (e.g., coordination complex, electrostatic binding, covalent coupling, and biospecific conjugation) between the target analytes and ligands. The association between a single core nanoparticle and analytes is rerecognized with satellite particles in the second step, which results in the coupled plasmon "core−satellites (COSA)" structure (Figure 1).

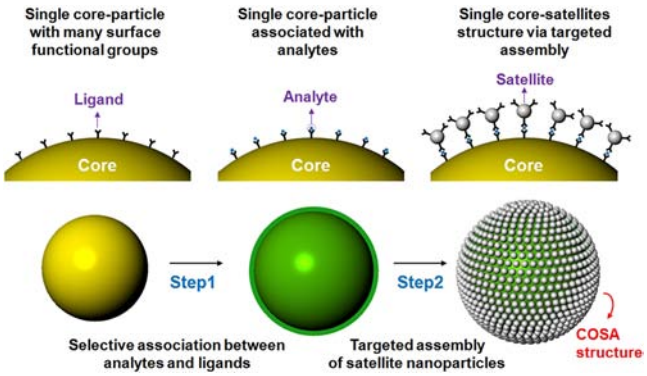

Figure 1. Schematic diagram for the formation of COSA nanoassembly. The method involves two steps including the selective recognition of targets with core nanoparticle and targeted assembly with satellite nanoparticles. The first step involves the exposure of a core nanoparticle with specific ligands to analytes to induce selective associations between target molecules and ligands. This association between a single core nanoparticle and analytes is rerecognized with satellite particles in the second step, which results in the formation of coupled plasmon COSA structures.

As a proof-of-concept demonstration of our COSA assembly and its sensing capability, a single 50 nm gold "core" particle linked by metal ions to 2.6 nm silver "satellite" particles (Figure 2a), was chosen for the following reasons. First, nanoparticles are usually synthesized by stabilization with a reducing agent (i.e., citric acid) with carboxylated (COO^-) moieties, which have a high affinity for most metal ions by forming metal−carboxylate complexes.[24] Our approach without complicated surface modification chemistry significantly simplifies the satellite assembly. Second, a 50 nm diameter gold particle, as a core, provides an excellent platform with multiple coordination sites for metal ions (e.g., a 50 nm gold particle can tether approximately 640 ± 80 thiolated ligands on its surface[25]), which could lead to high density satellite assembly. In addition, gold nanoparticles play a better role than silver, because a 50 nm core gold particle has green scattering color in terms of sensing application, which is the most sensitive color to the human eyes as compared to the 50 nm silver particle with a dim blue scattering color. Last, as satellites, 2.6 nm silver

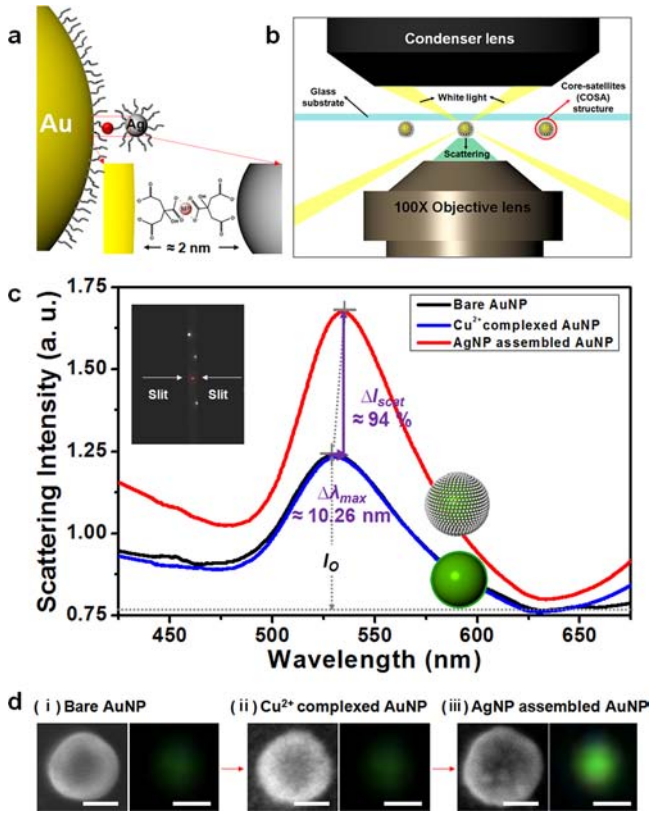

Figure 2. Proof-of-concept investigation of the COSA nanoassembly. (a) Description of the formation of metal ion complexes on the surface of particles. The gold nanoparticle (AuNP) was exposed to a 10 μM Cu^{2+} solution, and then was treated with silver nanoparticles (AgNPs) to form a COSA structure via Cu^{2+} sandwiched linkage (COO^-−Cu^{2+}−^-OOC), which is approximately ∼2 nm. (b) Microscopic configuration for collecting Rayleigh scattered light from a single COSA structure. (c) Representative scattering spectra. A single bare AuNP (black), a Cu^{2+} complexed AuNP (blue), and a core (AuNP)−satellites (AgNPs) structure formed by treatment of 10 μM Cu^{2+} (red). Inset indicates the single core captured by moving to the center and closing an adjustable entrance slit. (d) Electron micrograph (left) and dark-field image at each step (right): (i) Bare AuNP, (ii) Cu^{2+} complexed AuNP, and (iii) AgNPs-assembled AuNP. Scale bars for electron micrographs and dark field images are 25 and 500 nm, respectively.

particles (see Figure S1 in the Supporting Information) perform excellent roles in inducing tunable plasmon coupling according to the amount of the complexed target metal ions, because they are sufficiently small that their binding to the core can be directly correlated with the amount of target metal ions.

Figure 2 shows typical characteristics of our approach. First, Cu^{2+}, among metal ion species, was used here because it is not only of analytical significance in biological and environmental processes[26,27] but also is the most responsive metal ion for COO^- moieties (see Figure 2a).[24] One moiety among 3 carboxylate (COO^-) moieties in a citrate on the gold core particle is first bound to a Cu^{2+} ion where it is followed by binding of COO^- on the silver satellite. Consequently, the Cu^{2+} is chelated by the two COO^- moieties within two citrate ligands on the core and satellite nanoparticle, as shown in the inset of Figure 2a.

To confirm the interaction between Cu^{2+} ions and citrate moieties, we measured the color changes (Figure S2(a)) and UV−vis spectral changes (Figure S2(b)) of gold and silver

dx.doi.org/10.1021/ja302684w | J. Am. Chem. Soc. 2012, 134, 12083−12090

colloid solutions after the addition of Cu^{2+} ions. First, we observed the color changes of the solutions, which were red to violet (1 to 2) and yellow to brown (5 to 6), respectively. Also, their corresponding UV−vis spectra show the decrease and red-shifts of their initial characteristic peaks by the Cu^{2+}-induced aggregation. Second, to further certify the formation of the Cu^{2+}−citrate complexes, we additionally performed identical experiments with gold nanoparticles coated with other functional groups (i.e., amine). We prepared the gold nanoparticle coated with poly(allylamine hydrochloride) [PAH], which has abundant amine (NH_2^+) moieties. Figure S2(c) shows the change in zeta potential (ζ-potential) of the nanoparticles from −40 to 40 mV by coating with PAH. In the case of PAH-coated gold nanoparticles, no significant color change and UV−vis spectral change (3 to 4) are observed, which clearly shows the citrate specific complexation of the Cu^{2+}. Furthermore, dynamic light scattering (DLS) measurements of the solutions before and after addition of Cu^{2+} ions show the remarkable increase of the particle size by the aggregation in the case of the citrated gold nanoparticles (Figure S2(d)). On the other hand, the PAH-coated gold nanoparticle shows no significant increase of their size. It was approximately 10 nm due to the thickness of PAH coating (Figure S2(e)).

In our study, for the direct observation of plasmon coupling, the changes in Rayleigh scattering images and spectra of a single plasmonic probe at each step were collected using a dark-field microscope (Figure 2b) with a true color imaging camera and a spectrometer with an adjustable slit to capture only a single nanoparticle (an inset of Figure 2c). The dark-field microscope technique combined with the use of a spectrometer has been widely utilized to characterize a single plasmonic nanoparticle,[9,10,12−14] and details of our setup have been described in our previous report.[9] In a typical experiment, a particle was illuminated with white light, and the Rayleigh scattered light from an individual particle was collected by a dark-field microscope in transmission mode (Figure 2b).

For the use of a single gold nanoparticle as a plasmonic probe, the single nanoparticles must be well-dispersed on a glass slide. To effectively immobilize nanoparticles, we fabricated a phase-separated self-assembled monolayer composed of two different organosilanes,[28] which are 3-aminopropyltriethoxysilane (APTES) and octadecyltrichlorosilane (OTS). The prepared layer results in the formation of amine (NH_2)-functionalized regions with a high affinity for gold nanoparticles and methyl (CH_3)-functionalized regions to prevent individual particles from coming into close contact with one another,[28] respectively. In addition, the passivation of the background areas using CH_3 moieties is important, in that it prevents metal ions from binding to the remaining areas, which are not occupied with gold nanoparticles.

The intrinsic resonant scattering peak of a single gold particle of 50 nm, that had been immobilized on a glass slide, was recorded at around 530 nm (see the black spectrum of Figure 2c), and its scattering color was dark green (right image of Figure 2d(i)). Upon exposure to a 10 μM Cu^{2+} solution, the resonant scattering peak of a single nanoparticle was slightly red-shifted (1.36 ± 0.189 nm) due to the dielectric environment change by the formation of Cu^{2+} complexes on the nanoparticle surface (see the blue spectrum of Figure 2c), but its intensity was almost the same as that of the original spectrum (black spectrum). Thus, no change in the scattering color was observed (right image of Figure 2d(ii)). However, after treatment with silver nanoparticles, substantial changes in both the position of the peak and its intensity ($\Delta\lambda_{max}$ and ΔI_{scat}, see the red spectrum of Figure 2c) were observed, as evidenced by a red shift of 10.26 ± 0.195 nm and a 94% enhancement in scattering intensity, as compared to the initial spectrum of the bare gold core particle. We attribute this to significant enhancement in the plasmon coupling as a result of COSA assembly. Because of the drastic peak shift, it is possible to easily observe changes in scattering color, from a dark green (right images of Figure 2d(i) and (ii)) to a bright green color (right image of Figure 2d(iii)). The formation of a COSA assembly was also confirmed by a scanning electron microscope image showing that the surface of the core particle is decorated with small nanoparticles (left image of Figure 2d(iii) and Figure S3 in the Supporting Information). In contrast, Figure S4 (Supporting Information) shows that the addition of silver nanoparticles to the core gold nanoparticle lacking Cu^{2+} linker resulted in a minimal change in spectrum (i.e., 0.26 nm shift and an 8.6% enhancement). Moreover, the scanning electron microscope image obtained from this control sample shows no assembly of the silver satellites on the core gold nanoparticle (Figure S3(a) in the Supporting Information). These results clearly indicate that the scattering peak shift we observed results from the targeted assembly of silver nanoparticles on the core gold nanoparticle.

Having experimentally demonstrated the COSA assembly and corresponding plasmonic characteristics, we then investigated the tunability of COSA optical response in a quantitative manner by performing simulations. To calculate the LSPR scattering spectrum of a single COSA structure, we used the coupled discrete dipole approximation (DDA) method.[29] Spectral simulations were carried out using a structural model consisting of a single 50 nm core gold particle evenly surrounded by 2.6 nm silver satellite particles with an interparticle distance of 2 nm (the approximate length of the COSA linker, Cu^{2+} sandwiched between two citric acid moieties, used in the system), by increasing the number of satellites (0, 140, 280, 420, and 560). Figure 3a shows that the assembly of plasmonic satellites around a plasmonic core induces significant spectral shifts in both wavelength and intensity. As the number of satellites increases, we observed not only nearly a linear red shift in wavelength (Figure 3b) but also

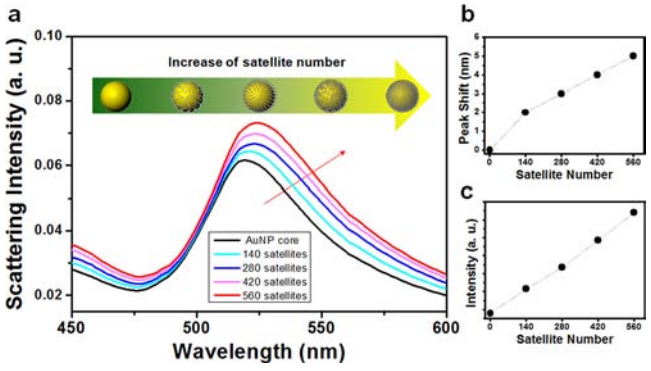

Figure 3. Spectral simulations for the COSA nanoassemblies as a function of increasing number of satellites. (a) Simulated scattering spectra for 50 nm AuNP cores assembled with different numbers (0, 140, 280, 420, and 560) of 2.6 nm AgNP satellites. (b) The plot of scattering peak shift with increasing number of satellites. (c) The plot of scattering intensity with increasing number of satellites.

dx.doi.org/10.1021/ja302684w | J. Am. Chem. Soc. 2012, 134, 12083−12090

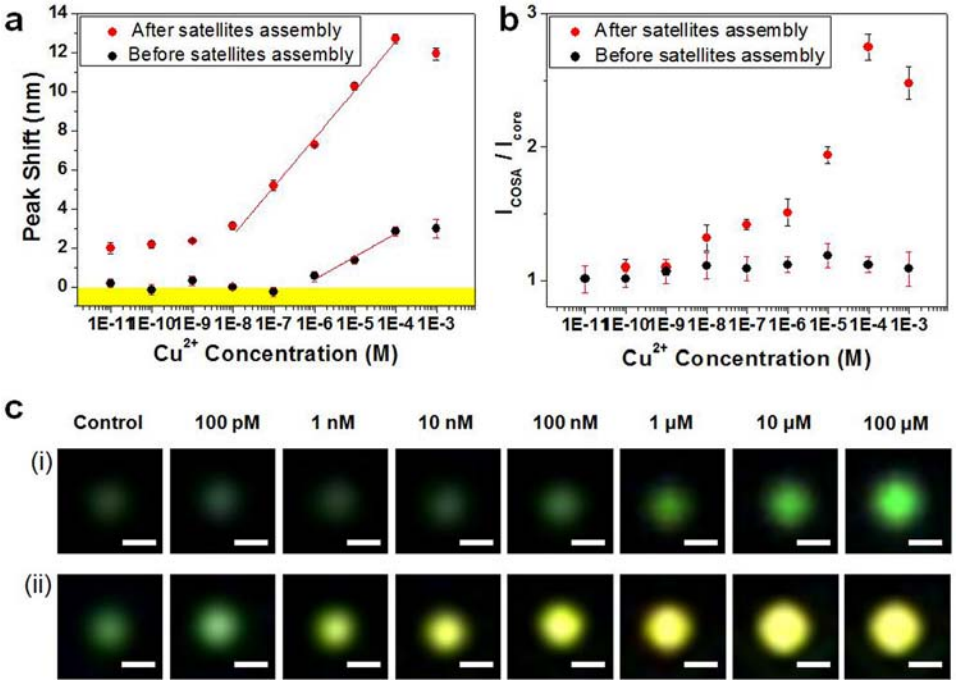

Figure 4. Quantification of optical responses achieved by the COSA nanoassembly as a function of increasing Cu^{2+} concentrations. (a) Plots of peak shift for a COSA assembly (red dots, after satellites assembly) and a control (black dots, before satellites assembly) in the range from 100 pM to 1 mM. The red lines are semilogarithmically fitted to the Cu^{2+} concentration data points. Error bars were included on all dots. The regression coefficient (R^2) is 0.995 (upper plot) and 0.974 (lower plot), respectively. A yellow box indicates the below region of the spectral resolution (0.26 nm). (b) Plots of the ratio of the increased scattering intensity from the original intensity of core (I_{COSA}/I_{core}) for a COSA assembly (red dots) and a control (black dots) as a function of Cu^{2+} concentration. Error bars were included on all dots. (c) Dark-field scattering images at each Cu^{2+} concentration for (i) a dark green probe and (ii) a bright green probe. Images were taken before (control) and after the assembly of satellites linked by Cu^{2+} (100 pM to 100 μM). Scale bar is 500 nm.

a linear increase in intensity (Figure 3c), in the simulated scattering spectra, demonstrating tunability of optical response. Considering that most plasmonic detection methods have utilized wavelength shift as an optical response,[3−5,8−10,14] this finding provides additional capability to potentially utilize intensity change as optical signals.

To evaluate the reliability of the COSA nanoassembly and utilize it as a sensing principle, we experimentally collected scattering spectra with increasing Cu^{2+} concentration. A single 50 nm particle as a core, as judged by its color and scattering peak (dark green and $\lambda_{max} \approx 530$ nm, see the 10 white circles in the left image of Figure S5a), was selected as a probe. Each spectrum recorded from 10 particles was presented in Figure S5b (Supporting Information). The reliability of single gold nanoparticle spectral shift occurred by Cu^{2+} ion exposure, and subsequent satellite assembly was examined and justified by minimal standard deviation of the spectral shift from 10 different particles (Figure 4a and b). Because the spectral resolution of our detection system is 0.26 nm,[9] it is possible to distinguish minute signal differences arising from a single core particle, as shown in the standard deviation of the lower plot (black dots) in Figure 4a. Notably, the introduction of a Cu^{2+} complex on the surface of a single core particle followed by the targeted assembly of silver satellite particles enabled larger peak shift and intensity increase for all of the measured concentration range (Figure 4a and b), consistent with the earlier observation (Figure 2), demonstrating reliability of the assembly and its optical response.

Furthermore, with increased concentration of Cu^{2+} ions, we observed an increase in both peak shift and change of intensity (Figure 4a and b) and stronger dependence after the COSA nanoassembly. As shown in the upper (red dots) and lower (black dots) portion of Figure 4a, the peak shift systematically increases to a longer wavelength with increasing Cu^{2+} concentration from 10 pM to 100 μM and from 1 μM to 100 μM, respectively. As compared to the control spectrum (0.26 nm shift in Figure S4), we observed significant peak shifts (2.16 $\pm$ 0.195 and 2.34 $\pm$ 0.050 nm, respectively) in the scattering spectra generated from COSA assemblies, even for concentrations of 100 pM and 1 nM. These shifts are sufficient to identify the presence of Cu^{2+}, which indicates a low limit of detection by using a COSA assembly-based sensor. We note that the limit of detection has been determined as 1 nM due to a relatively large standard deviation in the picomolar concentration range. In the case of single core particle probe (without satellites), no significant peak shift (<0.26 nm, indicated by the yellow box) was observed below the concentration of 1 μM. Collectively, Cu^{2+} sensing based on our coupled plasmonic core−satellites enabled at least 1000 times better detection limit as compared to that of a single plasmonic nanoparticle. In the range from 10 nM to 100 μM, a plot of scattering peak shift versus Cu^{2+} concentration of COSA assemblies shows a linear fit, with a regression coefficient of 0.995 (semilog scale). It is noteworthy that individual single COSA probes registered substantial shifts of 3.12 $\pm$ 0.195 nm after exposure to concentrations of Cu^{2+} as low as 10 nM. This response is considerably larger than those of all spectra obtained over the entire concentration range using only a single core particle with no satellites attached (black dots). As confirmed by the spectral simulations, when the satellites were

dx.doi.org/10.1021/ja302684w | J. Am. Chem. Soc. 2012, 134, 12083−12090

assembled on the core particle, the scattering intensities (I_{COSA}/I_{core}) also drastically increased as a function of Cu^{2+} concentration, whereas the single core system failed to induce any significant change (Figure 4b). Consequently, it can be concluded that the enhancement in intensity as well as the peak shift is also reliable when a COSA assembly is used as a sensing principle. After 100 μM, the signals did not increase any more. We think that 100 μM would be a critical point to allow the maximum signal change. Interestingly, over the concentration range of 100 μM, both signals (peak shift and intensity) slightly decrease, which is probably due to the silver shell-like characteristics of the close-packed silver satellites on the gold core. We note that the blue-shift of the UV extinction (i.e., absorbance and scattering) spectrum typically occurred (please also refer to references), in the case of the Au core−Ag shell structures.[30−33]

Our observed peak shift and intensity increase can be attributed to strong plasmon coupling between a core and satellites. The observed red shift of peak wavelength in our gold core and silver satellites nanoassemblies can be understood as a result of polarization of silver satellites at gold core resonance frequency.[34] In addition, the intensity increase in our nanoassemblies is consistent with the wavelength dependence of gold loss levels as the peak red-shifts, together with dielectric environment changes[19,34] due to silver satellites and metal ions. We would like to point out that the environment effect due to metal ions and citrate moieties, which was not taken into consideration in our simulation, could have caused the discrepancy between the intensity increment of the simulation (Figure 3) and the experiment (Figure 4a and b).

In a similar way, the peak shift in the case of gold core and gold satellites can be achieved by implementing a similar assembling approach. Our simulation of scattering spectra of gold or silver satellites on a gold core (see Figure S6 in the Supporting Information) revealed that gold satellites induced a stronger red shift than did silver satellites, which is consistent with earlier studies.[34] In terms of scattering intensity, silver satellites induced larger enhancement than gold satellites. This indicates that the optical signal can be easily tuned by adjusting the composition as well as size and number of the satellites[23] depending on the sensing purposes. It should be noted that it is difficult to distinguish the difference in the quantity of the bound targets in the case of the core−shell structure because the optical properties of the core−shell structure can be usually tuned by the thickness of shell.[30−33] We have additionally tried to induce the Cu^{2+}-linked nanoassembly of big silver satellites (i.e., 10 nm) to the 50 nm gold nanoparticle. At the same high Cu^{2+}concentratration of 100 μM, the very low density of 10 nm silver satellites was decorated on the 50 nm core gold nanoparticle, as compared to the high density decoration of 2.6 nm silver satellites to the core particle in our typical observation (see Figure S7 in the Supporting Information). Taking into consideration our concept for the targeted assembly of the satellites to "single" core particle in accordance with binding quantity of the targets to the core particle and its corresponding spectral change, we would like to note that the high-density assembly of small satellites to the single core nanoparticle is a more suitable choice to quantification of the target than both the assembly of large satellites to the core and the core−shell type within the dynamic concentration range.

Scattering intensity increase and peak shift after satellite assembly can also be seen by color changes through dark-field microscopic images (Figure 4c). The recorded increases in scattering intensity and peak shift are closely related to the increased brightness and changed color in the image for each single plasmonic probe. Even if we only selected the dark green probes and measured their spectra, it would be useful to show that the resulting color changes of probes are dependent upon their initial scattering colors. As the Cu^{2+} concentration increases, remarkable changes in the scattering color, from initial dark green and bright green (control) to bright green and yellow (exposure of Cu^{2+}), respectively, were observed after assembling satellites (see also Figure S5 in the Supporting Information). We further present the field of view of a larger area (88 μm × 66 μm, see Figure S8 in the Supporting Information) showing the changes in all probes after satellite assembly, which indicates that the method is highly reliable. We note the difference in the brightness at an initial state (i.e., dark green or bright green) can be attributed to the difference in sizes of the gold nanoparticles used as cores, which is inevitable in the case of synthesized nanoparticles (see also Figure S9 in the Supporting Information). These findings also suggest that such a colorimetric sensing probe with high spatial and temporal resolution would be applicable to the monitoring of the local environment around individual nanoplasmonic probes.

To explore the capability of COSA assembly to other ions, we also studied and compared the affinity of binding between ligands and metal ions for eight environmentally and biologically relevant metal ions (Cu^{2+}, Ni^{2+}, Ca^{2+}, Mg^{2+}, Fe^{2+}, Mn^{2+}, Na^{+}, and K^{+}) at the same ionic concentration, 10 μM. Figure 5a shows representative scattering spectra before (black) and after (red) COSA nanoassembly to various metal ions. On the basis of 10 spectra collected for each metal ion solution, we performed statistical analysis and summarized results demonstrating distinguishable wavelength shift (Figure 5b) and intensity increase (Figure 5c) after exposure to metal ions and subsequent satellite assembly. For the two signals, Cu^{2+} induced the most striking changes, which can be attributed to its high affinity for the carboxylated moiety among the various metal ions tested. It should be noted that the results show nearly the same trends for divalent metal ions ($Cu^{2+} \gg Ni^{2+}$, Ca^{2+}, $Fe^{2+} > Mn^{2+}$, Mg^{2+}), and the values were precisely consistent with the order of binding strength between citric acids and the metal ions.[24] Our experimental result at 10 μM, which is quite below the U.S. Environmental Protection Agency (EPA) regulation level (~20 μM, 1.3 ppm), clearly shows the remarkable differences between Cu^{2+} and other metal ions of more than 4 nm (i.e., 10 nm vs 6 nm) and 3 times (94% vs 30%) in terms of the peak shift and the % of intensity increase, as shown in Figure 5b and c. Consequently, the measured values are satisfactory to detect Cu^{2+} among other metal ions by color and brightness change (Figure 5d). The preferential complexation of Cu^{2+} to the COO^{-} moiety, as the result of the stronger affinity between them than that of other metal ions to the COO^{-} moiety, was also checked with mixtures equivalently containing various metal ions at a concentration of 10 μM. As shown in Figure S10, the peak shift for a mixture solution of all eight metal ions nearly corresponded to that of a 10 μM Cu^{2+} solution, and the intensity was also comparable, whereas the response for a mixed solution without Cu^{2+} was relatively small.

On the basis of our observation, we are currently investigating new experimental approaches derived from this sensing principle to develop simple on-chip colorimetric sensing methods via assembled arrays of COSA structures by controlling their density (see Figure S11 in the Supporting Information). We believe that the demonstrated strategies are

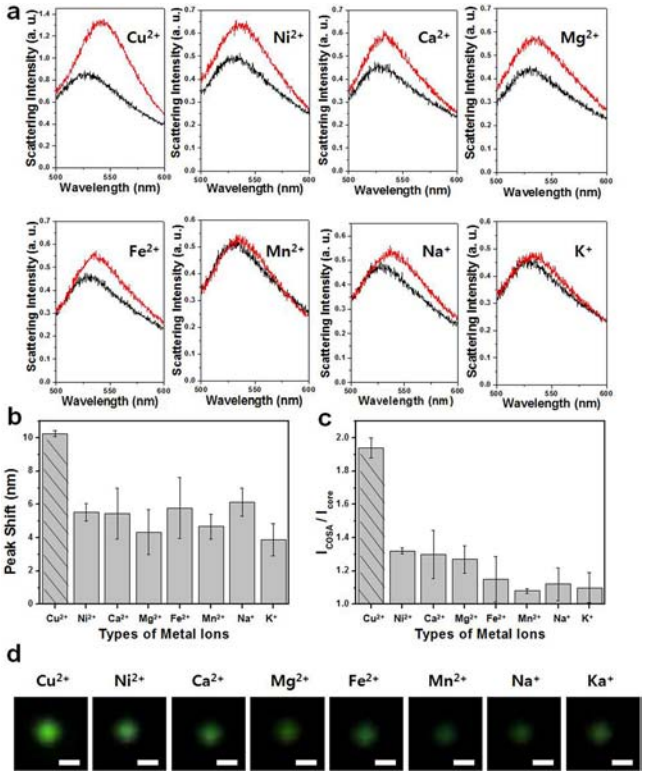

Figure 5. Optical responses for various metal ions measured with the COSA nanoassembly. (a) Representative scattering spectra before (black) and after (red) COSA nanoassembly at the same metal ions concentration of 10 μM. (b) Peak shifts after exposure to various metal ion solutions and subsequent AgNPs treatment. (c) Intensity enhancement after assembling COSA structure using various metal ion solutions. Bar graph summarizing the change in response to eight environmentally and biologically relevant metal ions (Cu^{2+}, Ni^{2+}, Ca^{2+}, Mg^{2+}, Fe^{2+}, Mn^{2+}, Na^{+}, and K^{+}). Error bars correspond to standard deviations measured from 10 probes. (d) Representative dark-field scattering images of individual single nanoprobes after exposure of different types of metal ion solutions. Scale bar is 500 nm.

highly feasible for combining current techniques to allow a programmable array of nanostructures and desirable molecular recognition. Well-arrayed COSA structures offer platforms in which plasmon coupling can be more strongly modulated and more easily detected. Above all, desirable molecular recognition is highly achievable using well-established conjugation chemistry (i.e., metal chelating moiety/metal ions,[13] metalloprotein/metal ions,[35] biotin/streptavidin,[36] antibody/antigen,[37] and complementary oligonuleotides[38]). Therefore, the proposed strategies provide an extremely promising platform to allow highly versatile sensing methods for biologically and environmentally relevant analytes.

CONCLUSIONS

We have for the first time experimentally and systematically observed the optical signals that are enhanced by plasmon coupling, modulated in a single COSA nanoassembly. The complexation of metal ions to the surface ligands surrounding core and satellite nanoparticles resulted in COSA nanoassembly, and such nanoassemblies induced enhancement of plasmon coupling (i.e., intensity amplification and apparent spectra shift) in a single particle level. These propensities of plasmonic enhancements were also supported by simulation results using a theoretical model by increasing the number of satellites decorated on a single core. We also demonstrated metal ion sensing based on our coupled plasmonic core–satellites, which enabled at least 1000 times better detection limit as compared to that of a single plasmonic nanoparticle. The sensitivity of our system, using a single COSA structure, provides a highly promising principle for the development of novel detection methods for various biological and chemical analytes by substituting target specific ligands and controlling interstructural distances.

EXPERIMENTAL SECTION

Materials. Gold nanoparticles (AuNPs, 50 nm in diameter) were purchased from BBI international, Inc. 3-Aminopropyltriethoxysilane (APTES) and octadecyltrichlorosilane (OTS) were purchased from Sigma-Aldrich. Copper sulfate ($CuSO_4$) and other metal salts were purchased from Sigma-Aldrich. Silver nitrate ($AgNO_3$), sodium borohydride ($NaBH_4$), sodium citrate dehydrate ($Na_3C_6H_5O_7$ + $2H_2O$), and polyvinylpyrrolidone (PVP) were purchased from Sigma-Aldrich. All water used was purified to above 18 MΩ using a Milli-Q DI water system (Millipore).

Preparation of 2.6 nm Silver Nanoparticles (AgNPs). 2.6 nm silver nanoparticles were synthesized by following previously reported protocol.[39] Briefly, $AgNO_3$ (0.11 mM), sodium citrate (1.91 mM), PVP (0.052 mM), and H_2O_2 (25.0 mM) in 42.3 mL of DI water were mixed and stirred constantly. As $NaBH_4$ (150 μL, 100 mM) was added into the mixture, the solution color turned to light yellow. After being stirred for another 3 h, the solution was filtered using 0.2 μm membrane filters.

Immobilization and Functionalization of Single Gold Nanoparticles on a Glass Slide. Prior to the immobilization of single gold nanoparticles, glass slides were cleaned in a piranha solution (H_2SO_4:H_2O_2 = 7:3 v/v) for 1 h and followed by rinsing with DI water and drying in a stream of N_2. A cleaned glass slide was immersed in an ethanolic solution of 5 mM APTES and incubated for 10 min. The modified surface with APTES was sonicated in pure ethanol to remove excess reagents, followed by drying in a stream of N_2. The area undeposited by APTES on the glass slide was then passivated by the treatment with a 5 mM OTS in a toluene solution for 3 h. For the immobilization of single gold nanoparticles, 200 μL of a colloidal solution containing 50 nm spherical gold particles was dropped onto the modified glass slide. After 1 min, the gold nanoparticles physically deposited were washed with DI water, and the glass slide was dried in a stream of N_2.

Formation and Adjustment of Core–Satellites Structures. For the formation of core–satellites structures and adjustment of the number of satellites, a variety of concentrations of Cu^{2+} solutions were dropped onto the gold nanoparticles immobilized on the glass slide. After 1 h, the glass slide was washed with DI water and was dried with N_2. The prepared 2.6 nm silver particles solution was dropped onto the Cu^{2+} treated gold nanoparticles immobilized on the glass slide. Silver particle of 2.6 nm diameter was bound to each adsorbed Cu^{2+} ion on the gold nanoparticles. Silver nanoparticles surrounded on the surface of a 50 nm gold particle, and core (gold nanoparticle)–satellites (silver nanoparticles) structures were consequently formed on a slide glass. After 3 h, the core–satellites structures immobilized on a glass slide were washed with DI water and were dried in a stream of N_2. For the validation of target-specific (Cu^{2+}) selective formation of core–satellites structures, control experiments were also performed for several cases (i.e., only silver nanoparticles treatment without exposure to Cu^{2+}, and other metal ion solutions, such as Ni^{2+}, Ca^{2+}, Mg^{2+}, Fe^{2+}, Mn^{2+}, Na^{+}, and K^{+}).

Collection of Scattering Spectra from the Single Core–Satellites Structures. Each scattering spectrum after exposure of gold nanoparticles to various concentrations of Cu^{2+} (100 pM to 100 μM), followed by exposure to a silver nanoparticles solution, was measured. The initial scattering spectrum of a single gold nanoparticle immobilized on a glass slide was first obtained. After the treatment with metal ion solutions, individual scattering spectra of preselected single gold nanoparticles were collected. After silver nanoparticles

dx.doi.org/10.1021/ja302684w | J. Am. Chem. Soc. 2012, 134, 12083–12090

treatment, scattering spectra of preselected single core−satellites structures were also taken. For all data, the reliability of the observed spectral shift and intensity ratio from the single particle were examined by the standard deviation of the spectral shift from 10 different particles at the same condition. The intensity ratio (I_{COSA}/I_{core}) was calculated by dividing by the I_{scat} value of the core−satellites.

Discrete Dipole Approximation (DDA) Simulations. The scattering spectra of core−satellites nanostructure were calculated using the DDA method.[40] As depicted in the model structure, core gold nanoparticle of 50 nm diameter was located at the center of the coordinate system. Silver nanoparticles of 2.6 nm diameter were evenly distributed around the core nanoparticle at a fixed radius according to their number of satellites (0, 140, 280, 420, and 560). The distance between core gold nanoparticle and silver satellite particles is 2 nm (approximate length of the COSA linker, which is composed of metal ion plus two citric acid moieties as used in the system). For all DDA calculations, we used DDSCAT 7.0.7 code, which was developed by Drain and Flatau.[29] The interdipole separation was set as ca. 1 nm for the target nanostructure; therefore, approximately 80 000 dipoles were generated and used for the DDA calculation. For the calculation, the dielectric constants of gold and silver were obtained from the literature.[41]

■ ASSOCIATED CONTENT

Supporting Information

TEM image of 2.6 nm silver nanoparticles, citrate specific complexation of the Cu^{2+} ions, additional SEM images of the core−satellites assembled structures, control spectra for the probe treated without metal ions, 10 pairs of scattering spectra before and after COSA nanoassembly at 10 μM Cu^{2+}, simulation of scattering spectra of gold or silver satellites on a gold core, the large field of view showing the changes in all probes, characterization of a single gold nanoparticle and gold nanoparticles' solution, selective response for Cu^{2+} in mixed metal ion solutions, and the demonstration of a simple on-chip colorimetric sensing method. This material is available free of charge via the Internet at http://pubs.acs.org.

■ AUTHOR INFORMATION

Corresponding Author

jyi@snu.ac.kr; twkang@sogang.ac.kr

Present Address

[‖]Department of Bioengineering, University of California at Berkeley, Berkeley, California 94720, United States.

Author Contributions

[§]These authors contributed equally.

Notes

The authors declare no competing financial interest.

■ ACKNOWLEDGMENTS

This work was supported by grant no. 101-081-032 from the Ministry of Environment, Korea, and WCU (World Class University) program through the Korea Science and Engineering Foundation funded by the Ministry of Education, Science and Technology (R31-10013). This work was also supported by the National Research Foundation of Korea (NRF) grant funded by the Korea government (MEST) (no. 2011-570 0015749) and by a grant of the Korea Healthcare technology R&D Project, Ministry of Health & Welfare (Grant No. A103001).

■ REFERENCES

(1) Stewart, M. E.; Anderton, C. R.; Thompson, L. B.; Maria, J.; Gray, S. K.; Rogers, J. A.; Nuzzo, R. G. *Chem. Rev.* **2008**, *108*, 494.

(2) Camden, J. P.; Dieringer, J. A.; Zhao, J.; Van Duyne, R. P. *Acc. Chem. Res.* **2008**, *41*, 1653.

(3) Haes, A. J.; Van Duyne, R. P. *J. Am. Chem. Soc.* **2002**, *124*, 10596.

(4) Marinakos, S. M.; Chen, S. H.; Chilkoti, A. *Anal. Chem.* **2007**, *79*, 5278.

(5) Zhao, J.; Das, A.; Schatz, G. C.; Sligar, S. G.; Van Duyne, R. P. *J. Phys. Chem. C* **2008**, *112*, 13084.

(6) Kim, Y. J.; Johnson, R. C.; Hupp, J. T. *Nano Lett.* **2001**, *1*, 165.

(7) Lee, J. S.; Han, M. S.; Mirkin, C. A. *Angew. Chem., Int. Ed.* **2007**, *46*, 4093.

(8) Chah, S.; Hammond, M. R.; Zare, R. N. *Chem. Biol.* **2005**, *12*, 323.

(9) Song, H. D.; Choi, I.; Yang, Y. I.; Hong, S.; Lee, S.; Kang, T.; Yi, J. *Nanotechnology* **2010**, *21*, 145501.

(10) Nusz, G. J.; Marinakos, S. M.; Curry, A. C.; Dahlin, A.; Hook, F.; Wax, A.; Chilkoti, A. *Anal. Chem.* **2008**, *80*, 984.

(11) Liu, G. L.; Long, Y. T.; Choi, Y.; Kang, T.; Lee, L. P. *Nat. Methods* **2007**, *4*, 1015.

(12) Choi, Y.; Kang, T.; Lee, L. P. *Nano Lett.* **2009**, *9*, 85.

(13) Choi, Y.; Park, Y.; Kang, T.; Lee, L. P. *Nat. Nanotechnol.* **2009**, *4*, 742.

(14) Sonnichsen, C.; Reinhard, B. M.; Liphardt, J.; Alivisatos, A. P. *Nat. Biotechnol.* **2005**, *23*, 741.

(15) Pastoriza-Santos, I.; Gomez, D.; Perez-Juste, J.; Liz-Marzan, L. M.; Mulvaney, P. *Phys. Chem. Chem. Phys.* **2004**, *6*, 5056.

(16) Encina, E. R.; Coronado, E. A. *J. Phys. Chem. C* **2010**, *114*, 16278.

(17) Loweth, C. J.; Caldwell, W. B.; Peng, X. G.; Alivisatos, A. P.; Schultz, P. G. *Angew. Chem., Int. Ed.* **1999**, *38*, 1808.

(18) Chen, J. I. L.; Chen, Y.; Ginger, D. S. *J. Am. Chem. Soc.* **2010**, *132*, 9600.

(19) Sebba, D. S.; Mock, J. J.; Smith, D. R.; LaBean, T. H.; Lazarides, A. A. *Nano Lett.* **2008**, *8*, 1803.

(20) Sebba, D. S.; Lazarides, A. A. *J. Phys. Chem. C* **2008**, *112*, 18331.

(21) Pal, S.; Sharma, J.; Yan, H.; Liu, Y. *Chem. Commun.* **2009**, 6059.

(22) Waldeisen, J. R.; Wang, T.; Ross, B. M.; Lee, L. P. *ACS Nano* **2011**, *5*, 5383.

(23) Ross, B. M.; Waldeisen, J. R.; Wang, T.; Lee, L. P. *Appl. Phys. Lett.* **2009**, *95*, 193112.

(24) Mengel, K. *Principles of Plant Nutrition*, 5th ed.; Kluwer Academic Publishers: Dordrecht; Boston, 2001.

(25) Hill, H. D.; Millstone, J. E.; Banholzer, M. J.; Mirkin, C. A. *ACS Nano* **2009**, *3*, 418.

(26) Gaggelli, E.; Kozlowski, H.; Valensin, D.; Valensin, G. *Chem. Rev.* **2006**, *106*, 1995.

(27) Zhou, Q. F.; Zhang, J. B.; Fu, J. J.; Shi, J. B.; Jiang, G. B. *Anal. Chim. Acta* **2008**, *606*, 135.

(28) Choi, I.; Kim, Y.; Kang, S. K.; Lee, J.; Yi, J. *Langmuir* **2006**, *22*, 4885.

(29) Draine, B. T.; Flatau, P. J. *J. Opt. Soc. Am. A* **1994**, *11*, 1491.

(30) Banerjee, M.; Sharma, S.; Chattopadhyay, A.; Ghosh, S. S. *Nanoscale* **2011**, *3*, 5120.

(31) Wu, Y.; Jiang, P.; Jiang, M.; Wang, T. W.; Guo, C. F.; Xie, S. S.; Wang, Z. L. *Nanotechnology* **2009**, *20*, 305602.

(32) Shore, M. S.; Wang, J.; Johnston-Peck, A. C.; Oldenburg, A. L.; Tracy, J. B. *Small* **2011**, *7*, 230.

(33) Deng, J. J.; Du, J.; Wang, Y.; Tu, Y. F.; Di, J. W. *Electrochem. Commun.* **2011**, *13*, 1517.

(34) Sebba, D. S.; LaBean, T. H.; Lazarides, A. A. *Appl. Phys. B* **2008**, *93*, 69.

(35) Lee, S.; Choi, I.; Hong, S.; Yang, Y. I.; Lee, J.; Kang, T.; Yi, J. *Chem. Commun.* **2009**, 6171.

(36) Choi, I.; Kang, S. K.; Lee, J.; Kim, Y.; Yi, J. *Biomaterials* **2006**, *27*, 4655.

(37) Huang, X. H.; El-Sayed, I. H.; Qian, W.; El-Sayed, M. A. *J. Am. Chem. Soc.* **2006**, *128*, 2115.

(38) Nam, J. M.; Jang, K. J.; Groves, J. T. *Nat. Protoc.* **2007**, *2*, 1438.

(39) Huang, T.; Nallathamby, P. D.; Xu, X. H. N. *J. Am. Chem. Soc.* **2008**, *130*, 17095.

(40) Yurkin, M. A.; Hoekstra, A. G. *J. Quant. Spectrosc. Radiat. Transfer* **2007**, *106*, 558.
(41) Weber, M. J. *Handbook of Optical Materials*; CRC Press: Boca Raton, FL, 2003.